**Journal of Wind Engineering and Industrial Aerodynamics**
September 2023, Volume 240 Pages 105449 (14p.)
https://doi.org/10.1016/j.jweia.2023.105449
https://archimer.ifremer.fr/doc/00843/95465/

**Archimer**
https://archimer.ifremer.fr

# The assessment of a fast computational method in predicting the unsteady loads of vertical axis wind turbines undergoing floating motion

Rosado Hau Nidiana [1], Augier Benoit [1, *], Paillard Benoit [2], Trasch Martin [1], Matoug Camil [1]

[1] Ifremer, RDT Research and Technological Development, F-29280 Plouzané, France
[2] HydroQuest SAS, F-38240 Meylan, France

* Corresponding author : Benoit Augier, email address : Benoit.Augier@ifremer.fr

**Abstract :**

The low center of gravity and low center of thrust of Vertical Axis Wind Turbines (VAWT) are interesting characteristics when considering Floating-Offshore Wind Turbine (FOWT) application. The motion due to the floating platform adds extra complexity to the unsteady aerodynamics of VAWT. Hence, both numerical and experimental studies become very challenging. This paper focuses on the assessment of $T\ ubinesF\ oam$, a fast tool consisting of the actuator line method (ALM) embedded in OpenFoam. Then, instead the typical bladed-solved Navier–Stokes equations, the ALM inserts the blade forces into the field as body forces into the momentum equation. A modified version of the $turbinesF\ oam$ library that includes surge motion for multiple rotors has been evaluated by comparison with an experimental set of data from a twin-rotor performing surge in a wind tunnel. This paper includes the main equations describing the kinematics implemented in the numerical code, as well as a convergence analysis of mesh size, time step and surge cycles. The numerically predicted thrust forces agreed with the experimental results for both investigated tip speed ratios for the case with no surge motion. The numerical and experiment results including surge motion indicated a minimal influence of the surge motion for the cases evaluated here. The last verification using CFD computations from the literature showed that the $turbinesF\ oam$ tool properly captures the main features of the surge motion. This verified numerical method is a promising tool to understand the effects of geometrical parameters on the performance and the wake development of VAWTs farms in floating-offshore environments.

**Highlights**

► Fast numerical tool to predict loads for double VAWTs undergoing floating motion. ► Experimental data of a twin rotor with surge and with no surge motion. ► Capabilities and limitations in predicting unsteady forces under surge motion.

**Keywords** : Off-shore, Torque, CFD, Lowfidelity, VAWT

Please note that this is an author-produced PDF of an article accepted for publication following peer review. The definitive publisher-authenticated version is available on the publisher Web site.

**Nomenclature**

| | |
|---|---|
| $\alpha$ | Angle of attack |
| $\lambda$ | Tip Speed Ratio |
| $\nu$ | Kinematic viscosity |
| $\omega$ | Rotational speed |
| $\phi_s$ | Phase shift angle in surge motion |
| $\theta$ | Azimuthal angle |
| $c$ | chord length |
| $C_P$ | Power coefficient |
| $D_i$, $D_o$, $D_w$ | Distance from the domain center to the Inlet, outlet, and side walls. |
| $e_\theta$ | Unit vector normal to the blade tangential velocity |
| $e_c$ | Unit vector along the chord direction |
| $F_L$, $F_D$, $F_N$, $F_T$, $F_x$, $F_y$ | Lift, drag, normal, tangential, thrust and side forces |
| $H_z$ | Distance from the middle plane of the rotor to upper and bottom walls |
| $R$ | Radius |
| $Re$ | Reynolds number |
| $U_\infty$ | Incoming undisturbed wind speed |

## 1. Introduction

In the last years, many efforts have been made worldwide to implement strategies to achieve the target of a maximum global warming temperature of 1.5°. According to the Intergovernmental Panel on Climate Change, supplying electricity through zero or low-carbon sources represents a crucial pathway to mitigate the $CO_2$ emissions [1]. Therefore, the development and participation of renewable energies in the electricity market have been increasing. Solar and wind energy are the technologies with the largest amount of capacity installed around the world and, the projection for 2050 remains increasing [2].

The electricity production through wind energy technology is classified, accordingly to the location of the wind farms, in an onshore and offshore generation. At present, offshore wind energy contributes to a small percentage of the global electricity supply. Nevertheless, it has a huge potential due to the vast extent of the marine territory, the energetic density and steadiness of the offshore wind resource, and, less controversy with local stakeholders [3, 4].

The Horizontal Axis Wind Turbine (HAWT) is the dominant technology in both onshore and offshore applications. Because of the high maturity of the onshore HAWTs, the cost of electricity production is lower than the offshore applications and it is one of the most competitive in the electricity market [3]. To reduce the cost of the electricity generated by offshore technology, some approaches can be followed. For instance, by scaling current technology and implementing innovations or, by implementing new emerging technology [5].

Vertical Axis Wind Turbines (VAWTs) have some characteristics, such as the lower center of gravity, the location of the electric generator at the bottom of the rotor, and, a compact wake, that give them the potential as a cost-effective offshore wind turbine technology [6, 7, 8, 9]. However, the understanding of the VAWT performance becomes more challenging when operating on an offshore-floating platform; the six-degree of freedom (6 DOF) of the platform due to the movement of the waves, introduces many variables that affect might affect the performance and operation of VAWTs [10, 11].

Sandia Laboratories has developed the numerical tool called "Offshore Wind Energy Simulation (OWENS)" to perform the structural dynamics analysis of VAWTs. OWENS is able to perform an aeroelastic analysis of the rotor and to interact with other sub-modules: Hydrodynamic, mooring,

drive-train, and aerodynamic modules. Different VAWTs designs with a capacity of 5 MW were investigated and the main conclusion was that VAWTs have the potential to reduce the Levelized cost of electricity for the offshore wind energy [12]. Similarly, Cheng et. al. [13] investigated the structural dynamic response of three VAWT designs by using a simulation tool able to couple sub-modules that consider turbulent inflow conditions, aerodynamics, hydrodynamics, structural dynamics, the control system, and the mooring line system.

The 6-DOF motion can affect wake development. This has been confirmed by Lei et al. [14] by using computational fluid dynamics simulations (CFD) with a single rotor undergoing the pitch and surge motion. Also with CFD, Kuang et al. [15] investigated the impact of the pitching motion in the wake by using two rotors, one allocated behind the wake of the first rotor. Moreover, in order to understand the relation of the surge with the thrust force coefficient, a dynamic inflow model using an actuator cylinder method has been proposed by De Tavernier et al. [16]. Further, Lei et al. [10, 11] investigated with CFD, the effect on the power performance of a single VAWT due to the surge and pitching motions.

Despite that some efforts have been made until now in order to understand the effect of the 6-DOF in the wake, the power performance, and aerodynamic loads of a VAWTs, the knowledge and available tools to investigate the wake development for multiple rotors are very limited. Therefore, the main interest of this paper is to evaluate a fast method able to compute the aerodynamic loads and wake of multiple rotors but also, to include an offshore-floating platform motion. In this work, we focus only on the surge motion and we present first aerodynamic loads of an experimental twin-rotor undergoing surge and then, a numerical method is verified.

### *1.1. Review of methods*

Inherently, investigating the effect of the platform motion on the aerodynamic loads and wake of VAWTs requires three-dimensional numerical methods or experimental tests. Regarding experimental data, as far as the knowledge of the present authors, there is no available information in the literature that is useful for the objectives of this work. Despite that, some offshore VAWTs prototypes can be found commercially that might have some information [17]. Twin rotors without any 6-DOF motion have been tested in the wind tunnel and the results present wake and power coefficient data

[18, 19]. This lack of experimental data motivated our present experimental work described later.

Numerical simulations on VAWTs have become very common in the last few years. The most used approach consists of two-dimensional computational fluid dynamics (CFD) simulations [20] exploring the unsteady aerodynamics, wakes, parameters affecting the power performance, etc. Previous studies using 3D-CFD simulations to investigate the performance of VAWTs are presented in Table 1 and details of the number of blades, rotors, and mesh size are included. Regarding the double rotors or arrays rotor, investigations in 3D-CFD cover: the power performance of double a configuration and the effect of the spatial distance between both rotors [21]; the wake of double rotors [22]; the effect of a deflector in the power performance of a twin rotor [18]. Also, the effect of the backward distance between double rotors under the influence of a pitching motion was investigated with a CFD technique by Kuang et al. [15]. As it is observed from Table 1, investigating the VAWTs through 3D CFD requires a high computational cost and inclusive one-single rotor requires more than 4 million mesh elements. It is well known that using CFD allows us to obtain more in deep detail on the flow physics around the rotors and, for more specific aerodynamic research purposes this could be the best strategy.

The numerical method, the actuator line modeling (ALM), combines the advantages of the blade element method (BEM) with the capabilities of the CFD simulations to solve the Navier-Stokes (NS) equations at a low computational cost. The ALM methods first use the BEM to compute the corresponding forces on the blade element by using tabular data and then, using including these forces in the NS equations. This results in a method that does not require solving boundary layers but it does include the principal unsteady features present in the VAWTs. Also, the blade interaction and the wake are solved. The ALM has been employed to predict the performance of VAWTs in [31]. Bachant et. al. [32] developed a computational library for VAWTs by using OpenFOAM coupled with the ALM method, *turbinesFoam*. This method was validated by Bachant et. al. using the power coefficient curve of single rotors without any surge motion. Later, De Tavenier et al. [33] included the surge motion for a single rotor to predict some aerodynamic forces. Despite existing others, numerical methods, such as the actuator cylinder [34] with a very similar strategy used by the ALM, for the aim of the present research we select *turbinesFoam* since depicted to be an available free-numerical tool with some successful background for

Table 1: Numerical parameters for 3D VAWTs simulations

| Ref. | Config. | Blades | Floating motion | Model | Soft. | Mesh Elements |
|---|---|---|---|---|---|---|
| [23] | Single | 2 | No | $\kappa-\omega\ SST$ | Fluent | 2.95E6 |
| [24] | Single | 3 | No | $\kappa-\epsilon$ | Fluent | 9.5E6 |
| [25] | Single | 2 | No | SA | Fluent | 23.9E6 |
| [26] | Single | 1 | No | $\kappa-\omega\ SST$ | COSA | 90.0E6 |
| [27] | Single | 2 | No | $\kappa-\omega\ SST$ | Fluent | 1.4E6 |
| [28] | Single | 2 | No | $\kappa-\omega\ SST$ | Fluent | 3.8E6 |
| [29] | Single | 3 | No | LES | Fluent | 15.5E6 |
| [30] | Single | 2 | No | $\kappa-\omega\ SST$ | Fluent | - |
| [10] | Single | 3 | Surge | IDDES | Fluent | 4.7E6 |
| [11] | Single | 2 | Pitch | IDDES | Fluent | 4.5E6 |
| [22] | Double | 3 | No | LES | - | 1.85E12* |
| [18] | Double | 3 | No | $\kappa-\omega\ SST$ | Fluent | 3.9E6 |
| [21] | Double | 3 | No | LES | $STAR\ CCM+$ | 8.9E6 |
| [15] | Double | 3 | Pitch | LES | $STAR\ CCM+$ | 6.9E6 |

predicting power coefficient and to consider the surge motion with minor modifications. Other numerical tools such as CACTUS and QBLADE were investigated at the beginning of this project but the easier implementation of double rotor and surge motion in the ALM were the main reasons for the selection.

### *1.2. Outline*

As stated in the mentioned literature, there is an increasing interest in understanding the six degrees of freedom of the floating motion in the performance of VAWTs. Both subjects, double rotors, and floating motion showed a limited number of investigations. While experimental test on VAWTs in general represents a huge engineering challenge [35, 36, 37, 38], the CFD techniques also require high computational cost (see Table 1). Therefore, the ultimate intention of this research consists in obtaining a medium-high fidelity tool able to predict unsteady loads and the wake development of large counter-rotating VAWT rotors under floating-offshore environments. Thus, the present method would be able to consider multiple rotors undergoing surge motion.

This paper, firstly in Section 2 describes the main equations of the Kinematics in the VAWTs blades under surge motion. Section 3 described the experimental set-up and the twin rotor tested in the wind tunnel. A CFD case from the literature is also described since is used later for the verification process. Next Section 4 included the modifications to the *turbineFoam* library and a large numerical study on the mesh, domain, and time is carried out. Finally, the verification of *turbineFoam* for our double-rotor experimental test with surge motion is presented and discussed in Section 5.

## 2. Kinematics of the VAWTs blades

The rotating blades of a VAWT operating under a free-stream wind velocity $U_\infty$, perceive an actual wind flow frequently referred to as relative velocity ($U_{rel}$). Theoretically, neglecting any interference factor due to the presence of the rotor itself, the relative velocity depends on the vectorial result of the incoming flow velocity and the velocity of the blades $U_{blades}$ and, it is expressed as follows:

$$\vec{U}_{rel} = \vec{U}_\infty - \vec{U}_{blades} \tag{1}$$

Under a floating motion, in addition to the rotational speed on the blades, the full rotor experiences induced velocities due to the translation movements and the oscillations about its axis. As a result, the velocity of the blades needs to consider the induced velocities due to these six-degree movements.

For a VAWT rotating with an angular velocity, $\omega$, and performing a surge motion, the velocity of the blades ($\vec{U}_{blades}$) is given by the following expression:

$$\vec{U}_{blades} = \vec{U}_T + \dot{\vec{S}}_x \tag{2}$$

where $\vec{U}_T$ is the tangential velocity, and $\dot{\vec{S}}_x$ is the surge induced velocity.

Consider a clockwise rotation on the blades as illustrated in Fig. 1 and a coordinate system with $x$ positive in the same direction as the wind. A surge motion describing a sine function as expressed in Eq.(3), will induce a velocity in the blades given by Eq.(4) that results from the derivative of the given surge function.

$$s_x(t) = x_m sin(\omega_s t + \phi_s) \tag{3}$$
$$\dot{s}_x(t) = x_m \omega_s cos(\omega_s t + \phi_s) \tag{4}$$

$x_m$ is the amplitude of the surge and $\omega_s$ is the angular surge frequency.

The magnitude of the relative velocity and the angle of attack ($\alpha$) are the most important parameters to estimate the aerodynamic forces on a VAWT and hence, to predict the torque ($Q$) and the power of the rotor. Therefore, velocity vectors in Equations (1) and (2) need to be expressed in a second reference based on the blade motion position. This reference system consists of two unit vectors, $\hat{e}_c$ along the chord and, $\hat{e}_\theta$ towards the rotation axis, both indicated in Fig. 1.

The tangential velocity, $\vec{U}_T$, the surge induced velocity, $\dot{\vec{S}}_x$ and the inflow velocity $\vec{U}_\infty$ are expressed with the following equations:

$$\vec{U}_T = -\omega R \hat{e}_c \tag{5}$$
$$\dot{\vec{S}}_x = \dot{s}_x \cos\theta \hat{e}_c + \dot{s}_x \sin\theta \hat{e}_\theta \tag{6}$$
$$\vec{U}_\infty = U_\infty \cos\theta \hat{e}_c + U_\infty \sin\theta \hat{e}_\theta \tag{7}$$

where $\omega$ is the rotational speed of the blades, $R$ the rotor's radius and $\theta$ the azimuth angle of the rotor.

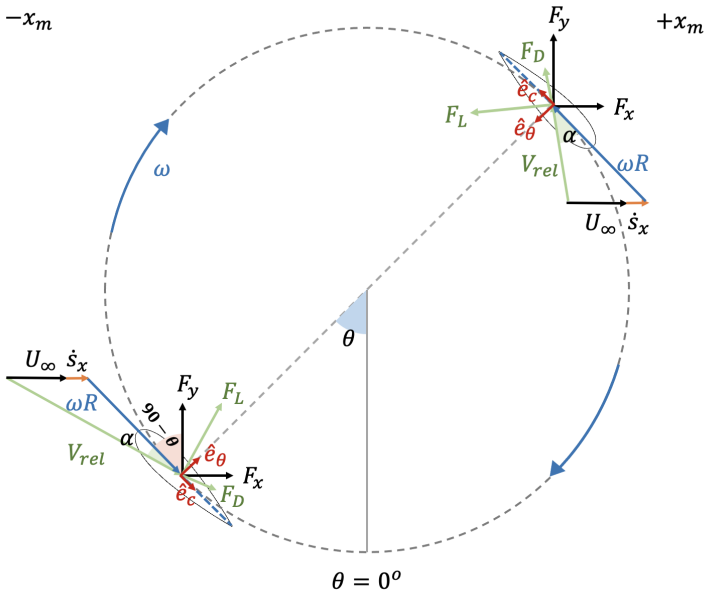


Figure 1: Velocities and forces present in a VAWT rotor performing a surge motion

The relative velocity in their components and magnitude is expressed as follows:

$$U_{rel,\hat{e}_c} = U_\infty \cos\theta + \omega R - \dot{s}_x \cos\theta \tag{8}$$

$$U_{rel,\hat{e}_\theta} = U_\infty \sin\theta - \dot{s}_x \sin\theta \tag{9}$$

$$|U_{rel}| = |U_{rel,\hat{e}_c}| + |U_{rel,\hat{e}_\theta}| \tag{10}$$

Finally, the angle of attack, $\alpha$, is defined as the angle formed by the relative velocity, $\vec{U}_{rel}$, and the chord. Therefore, using the components of the relative velocity, the angle of attack is calculated by next Eq.(11).

$$\alpha = \arctan\left(\frac{U_{rel,\hat{e}_c}}{U_{rel,\hat{e}_\theta}}\right) \tag{11}$$

The lift and drag forces, $F_L$ and $F_D$ respectively, are the aerodynamic forces on the airfoil. The lift is the generated force perpendicular to the relative velocity, and the drag is the parallel force. The radial force also called normal force $F_N$, is the resultant aerodynamic force towards the center

of rotation. The tangential force $F_T$ is the resultant aerodynamic force with a positive direction in the same rotating direction. $F_T$ directly influences the torque and the power generated by the rotor. The following equations describe $F_N$ and $F_T$ in terms of the lift and drag forces:

$$F_N = F_L \cos(\alpha) + F_D \sin(\alpha) \tag{12}$$

$$F_T = F_L \sin(\alpha) - F_D \cos(\alpha) \tag{13}$$

The thrust force, $F_x$, is the resultant aerodynamic force in the direction of the incoming free-stream wind speed $U_\infty$. The side force, $F_y$, also known as side-thrust force, is the resultant aerodynamic force perpendicular to the incoming flow velocity. Both forces are important for the structural turbine design and other supporting structures. The forces $F_y$ and $F_x$ are expressed as a function of the normal and tangential forces as follows:

$$F_y = F_N \cos(\theta) + F_T \sin(\theta) \tag{14}$$

$$F_x = F_N \sin(\theta) - F_T \cos(\theta) \tag{15}$$

The thrust coefficient, $C_x$, is given by Eq. 16, with $\rho$ the air density.

$$C_x = \frac{F_x}{0.5\rho\pi R^2 U_\infty^2} \tag{16}$$

The power coefficient is the ratio between the power generated about the axis of the rotor and the kinetic energy by the wind and it is typically computed with next expression:

$$C_P = \frac{\omega Q}{0.5\rho\pi A^2 U_\infty^3} \tag{17}$$

## 3. Cases of study

### *3.1. Experimental Study case 1: Wind tunnel twin rotor VAWT with surge and without surge motion*

All papers showing experiments must include a thorough formal experimental error analysis, including the errors in all measured variables and presented parameters, description of the instruments used, the way they are employed, calibration, etc.

A double counter-rotating rotor VAWT configuration has been tested under surge and without surge motion in a wind tunnel (Fig. 2). The

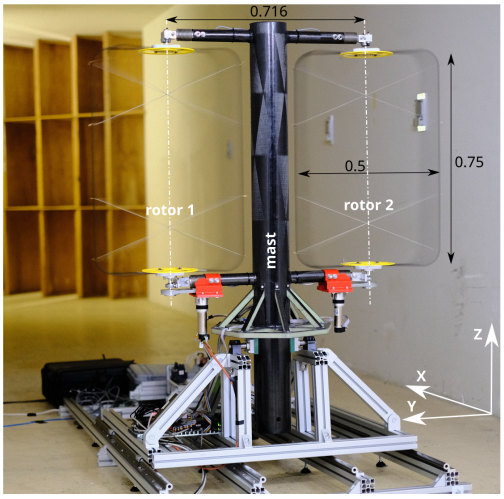


Figure 2: Experimental set-up of the twin-rotor VAWT model in the ISAE-ENSMA S620 wind tunnel. Dimensions are in meter.

Table 2: Geometrical parameters of the WindQuest twin-rotor wind turbine

| Airfoil | Diameter | Chord | Height | Contra-rotating direction |
|---|---|---|---|---|
| NACA0018 | 0.25 m | 0.0375m | 0.75m | Inwards |

experimental tests of the prototype were carried out in the ISAE-Ensma S620 wind tunnel. The two rotors are 0.75m high-0.5m wide and are composed of two blades of a constant NACA0018 section. The rotor parameters are presented in tab. 2. The wind tunnel section is 8.11 $m^2$ for a projected area of the model with actuators of 0.84 $m^2$. Both rotors are equipped by 1D load sensors measuring the thrust (X direction) located at the bottom and top pivot points.

A set of two actuators and assemblies is used to reproduce the motion of the floater on two Degrees of Freedom (DoF) and are illustrated in Fig. 2.The model is connected to a first sub-assembly trough a pivoting link at the bottom of the mast, simulating the pitch rotation This pitch assembly is placed, together with the rotor on a second assembly positioned on rails visible on Fig. 2), allowing for the translation on the Surge axis X. In the following study, only the surge motion will be considered.

The experimental setup allows to extract thrust force coefficient ($C_X$) as a function of the azimuth angle of the blades. Different configuration are tested exploring for the constant upstream speed of 5 $m/s$ five Tip Speed

Table 3: Geometrical parameters for the CFD case

| Airfoil | Diameter | Chord | Height | Pitch angle |
|---|---|---|---|---|
| NACA0021 | 2 m | 0.265m | 1.2 m | -8 ° |

Ratio (TSR) of 2.62, 3.14, 3.67, 4.19 and 4.71 with no surge motion and three TSR 2.41, 3.14 and 4.19 with surge motion tested under the range of frequencies of [0.46-1.93] - equivalent to a range of 8 to 20 revolution per surge period - and an amplitude range of [25-100] mm. Rotors have identical TSR for all considered configurations.

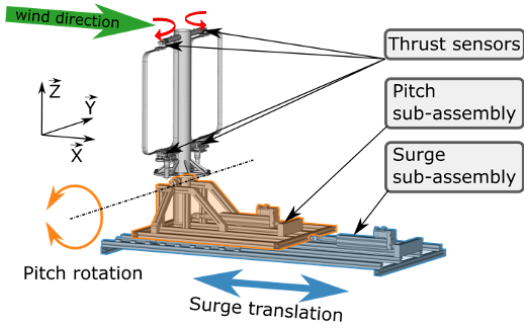


Figure 3: Description of the surge and pitch platforms system for the twin-rotor VAWT wind tunnel tests.

### *3.2. Numerical Study case 2: 3D CFD single rotor under surge motion*

A single VAWT with the geometric characteristics included in Table 3 has been investigated in [10] by using 3D CFD simulations. The surge motion investigated includes different amplitudes and frequency of surge. Here, the amplituded of 0.20 and 0.08 m with a period of surge equivalent of 4 times the period of the VAWT rotation are analysed. The tip speed ratio of the rotor is 1.82 and the wind speed of 8 m/s. This CFD case has been verified in the mentioned work and due to the main goals of this work, to verified a faster tool than a full CFD simulation, the overall equations implemented in TF are validated first with this case.

## 4. Method

### *4.1. TurbineFoam: the double rotor and kinematics of the floating motion*

TurbinesFoam, is a open library implemented in $OpenFoam$ (a free-source CFD software) and the simulation of the cross-flow wind turbines is done by using the actuator line element (ALM) to impose the virtual forces of the blades on the flow field and receiving communication with OpenFoam until convergence [39]. The corresponding blade forces are computed from static database of blades, corrected trough a dynamic stall model and then projecting these forces into the flow field and then update the velocity, $U$ and pressure $p$ quantities to compute the new inflow velocity as the time progress. Thus, reducing the number of cells since boundary layers are not solved. This method, take into account the unsteady lift and drag forces associated by nature with VAWT aerodynamics by using a dynamic stall model. Also, this method allows to collocate multiple VAWTs, and then, the double counter-rotating VAWT was easily implemented. More detail in the equations of this library can be found in [32]. In summary, the advantage of this approach is the reduction of the number of cells required to simulate a dual-rotor and to incorporate the surge motion.

Within this library, the $crossFlowTurbineAlsource$ is the responsible of defining the geometry of the VAWT blades, i.e, constructing and storing the geometric characteristics of the blades sections accordingly to the entrance in $fvOptions$. Including the surge motion leads to include: the surge motion of the actuator lines that actually needs to be move in position for a correct flow field forces projections and, the adequate calculation of the induced velocity due to surge and its finally effect in the relative velocity and angle of attack, both require for calculating the lift and drag unsteady forces. Both modification for the position and for the relative velocity has been made following De Taviener et al. previous code implementation [33]. With some further adaptations, the curvature effect has been taking into account and only influence by the rotation speed ($\omega$) and, multiple rotors with a metacenter of surge are added trough $fvOptions$. This surge motion implementation posses some initial limitations: for a rotor design where the chord-length changes, the initial local angle is not taking into account. A second limitation is when using the curvature effect, while using this only the Leishman-Beddoes dynamic stall model can be used. In TurbinesFoam then, the relative velocity per each section of the blades is calculated using Eq.(1) and the induced velocity of due to the surge is modified by adding this velocity vector on the blades

following expression Eq. (2). The new blade surge position is implemented trough the translation function available in the *actuatorLineElement* source code.

### *4.2. Numerical settings*

As mentioned before, the free CFD solver, OpenFoam v2016, is employed to perfom present simulations [40]. The full turbulence model $\kappa-\epsilon$ is selected. Within this model, the epsilonWallFunction is able to switch between the viscous and inertial sublayers [41]). The y+ is set to be 20, and this is withing the recommended work range of $[30-300]$ of the logarithmic layer. Since the ALM method is used to estimate the corresponding aerodynamic forces of the blades, thus no boundary layers are solved around the blades. Therefore, compared with most of previous CFD studies in VAWTs [42, 43], no transition method is required and this, leads to a decrease in the computational time.

Air transport properties were set to be: a kinematic viscosity $\nu = 1.48E-5\ m^2/s$, a density $\rho = 1.225\ kg/m^3$ and, a intensity of turbulence of $I = 0.2\%$.

The computational domain is depicted in Fig. 4 and it is formed by six faces: The distance from the center of the twin-rotor to the inlet, $D_i$; the distance from the center to the outlet, $D_0$; the distance from the center to the lateral domain sides, $D_w$ and, the distance from the center to the upper and lower domain sides $Hz$. Because the first experimental case was performed in an open wind tunnel and the second experimental test in a closed wind tunnel, the influence of the distance of the domain were investigated considering the sides, top and bottom faces with symmetry as boundary conditions. For the wind tunnel case, wall boundary conditions were applied and the distance was defined accordingly to the experimental information. For the other boundary conditions, and inlet velocity and an outlet pressure were imposed.

The mesh topology is illustrated in Fig. 4(b) and consists of a domain and two sub-domains. The subdomain 1 included the wake region of the rotor and the Sub-domain 2 including the near-region around the rotors. The settings and converge of the domain, mesh size and time step are discussed next.

### *4.3. Numerical converge analysis*

The dimensions of the base domain, $D_B$ were defined accordingly to the reviewed literature being of: $D_i = 5D$, $D_0 = 10D$, $D_w = 5D$ and, $Hz = 5.0H$. The snappyHexMesh method was employed to define the mesh size. In terms of the chord ($c$), the cell size in the outer domain was set to be

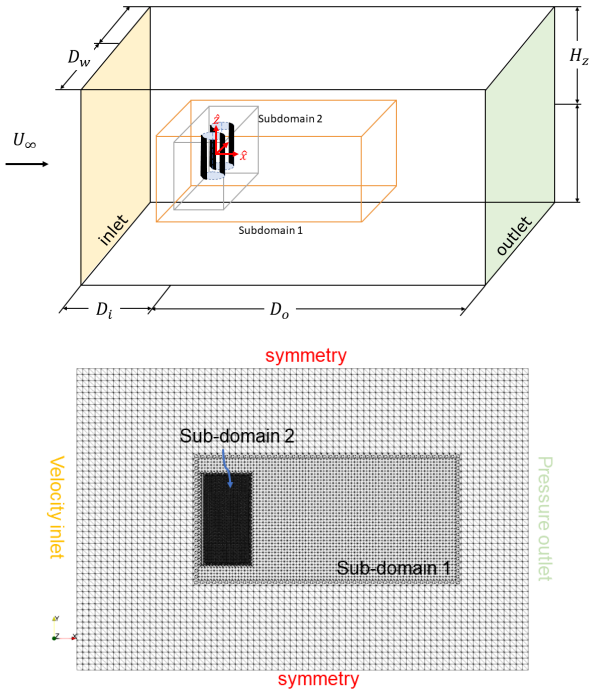


Figure 4: (a) Domain boundary conditions and (b) Mesh topology including the details of the subdomain mesh.

$2c$; the subdomain 1 has a cell size of $c$. Finally, the sub-domain 2 was evaluated with five cell sizes $2c, c, c/2, c/4$, and $c/8$, the mesh analysis with turbinesFoam has been also performed in [32] for a single rotor. The mesh analysis is included in Fig. 5 (a) and shows that a difference less than 17% is found when the cell-size is minor that $c/2$ with a number of total cells about $2.5E5$. The difference in the power coefficient using $c/4$ and $c/8$ cells size is minimal, but the increase in the number is 8 times lower. Present results are in agreement with findings in [32]. Therefore, a sub-domain with a cell size of $c/4$ represents the optimal size for the sub-sequenced simulations performed in this study.

To define the distances from the center to the sides of the domain, the base domain, $D_B$ was employed and then one single domain parameter, $D_w$ (lateral distance), $D_i$ (inlet distance), $D_o$ (outlet distance), and $H_z$ (top and bottom distances) was changed at the same time. Fig. 6 includes power coefficient as a function of the number of cycles for the evaluated domain parameters.

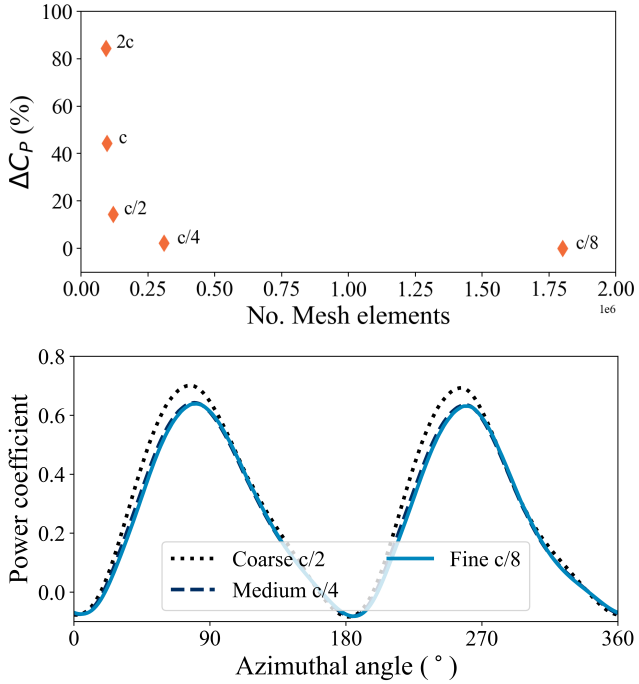


Figure 5: $\Delta\ C_P = (C_P - C_{P,c/8})/C_{P,c/8}$ (a) Difference in the power coefficient between each size-cell and the finest size $c/8$ at cycle 10th.(b) Power coefficient as a function of the azimuth angle for three cell sizes.

The inlet, $D_i = 2.5D$ and lateral, $D_w = 2.5D$ distances reduces the most the power coefficient. A value of $D_w = 7.5D$ showed very similar values to base case with $D_w = 5D$; in the same manner, increasing the inlet distance to $D_i = 7.5D$ gave the same result that the base domain with $D_i = 5D$. The outlet distance of $D_o = 7.5D$ and $D_o = 15D$ showed very similar results than the base domain with $D_o = 10D$. Finally, the distance $H_Z$ from the center to the top and bottom sides that showed very similar values were $H_Z = 5H$ and $7.5H$. Therefore, the simulation to be performed for the open-wind tunnel case have the next parameters: $D_i = 5D$, $D_o = 10D$, $D_w = 5D$ and, $H_Z = 5H$.

Time step independence study for simulation with VAWTs has been carried out on several previous work. Here, six values of time step were evaluated per one cycle of rotation: 2880, 1440, 720, 360, 240 and 180 time steps. These number of time steps correspond in term of azimuth degree step of: $\Delta\theta = 0.125°$, $0.25°$, $0.5°$, $1.0°$, $1.5°$ and, $2°$. Results included in Fig. 7 showed that

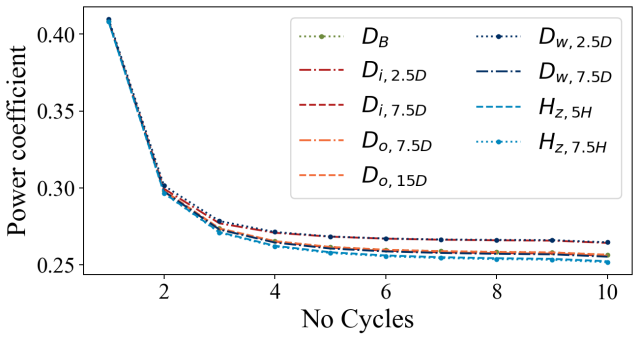


Figure 6: Influence of the domain distance parameters on the power coefficient as a function on the number of cycles.

at the cycle number 10, the variation of $C_P$ of each time step regarding the smallest time step case, 0.125° is lower than 4% for all the cases. The time step with $\Delta\theta = 0.5°$ exhibited less than 1% of difference and, $\Delta\theta = 0.25°$ and 0.125° was minimal. For the research purposes of the study a time step $\Delta\theta = 0.5°$ was selected.

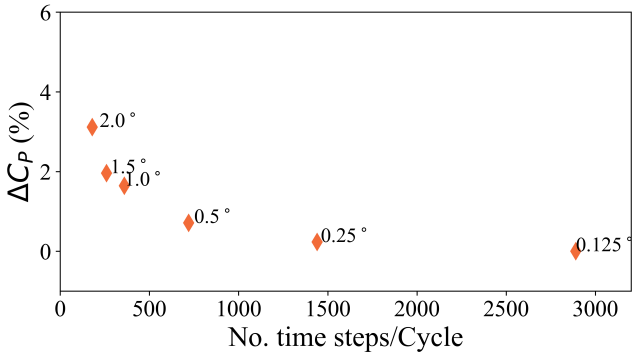


Figure 7: $\Delta C_P = (C_P - C_{P,0.125})/C_{P,0.125}$ Difference in the power coefficient between each time step and the smallest time step 0.125° evaluated at the 10th cycle.

Finally, to determine the number of surge periods, six period were compared. It was observed that from the second surge period the difference is minimal. This is attributed to the number of rotor cycles per surge; since more than several revolution of the rotor occurs when one surge finish, then convergence in surge is occurs very soon. For the cases investigated here, 3 surge periods employed.

## 5. Results and discussion

### *5.1. Thrust on the double rotor without surge*

The thrust forces for the twin rotor described in Section 3.1 were computed using the the numerical tool TF-OF and compared with our current experimental data. Two tip speed ratios were tested, $\lambda = 3.14$ and $\lambda = 4.71$ and the results are included in Fig.8. For both cases the forces predicted with the numerical tool showed a high agreement with the experimental measurements. For this two-bladed double VAWT the $C_T$ exhibited values close to zero at 0, 180 and 360 azimuthal positions. This is in agreement with previous experimental result with a two-bladed single rotor in [35] were the measurements on the thrust force increases with the increase of the tip speed ratio and showed zero values at the 0, 180 and 360 azimuthal position. The experimental curves were obtained by averaging 20 revolutions within intervals of 1 degree. As far as the knowledge of the present authors these experimental result on double rotor are the first with the instantaneous $C_T$ values.

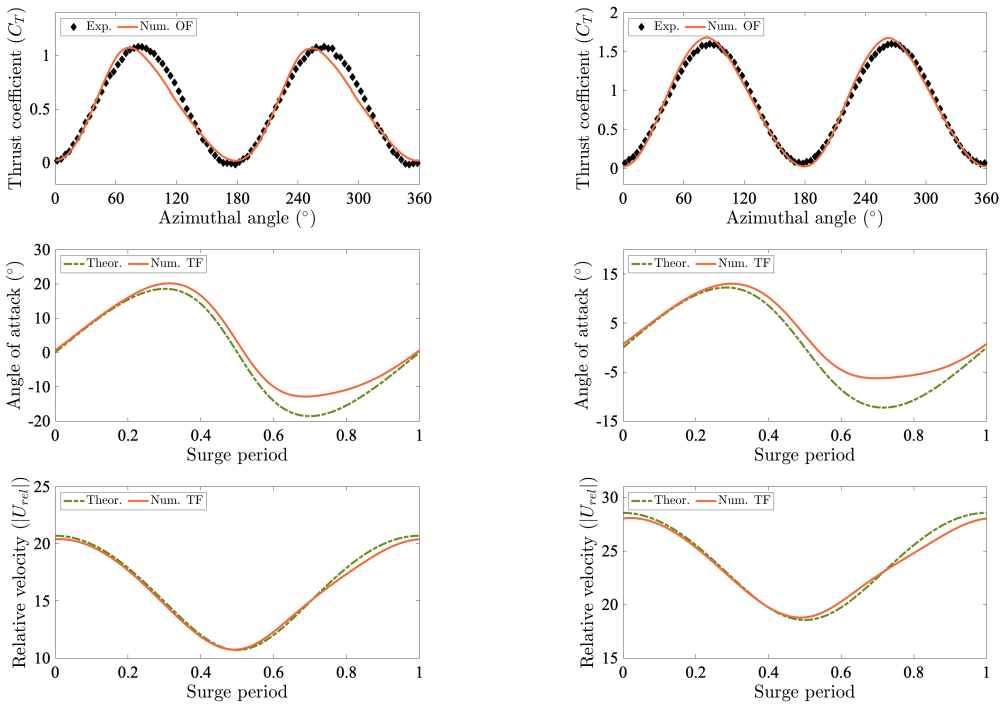


Figure 8: Thrust force coefficient for the twin rotor with (a) $\lambda = 3.14$

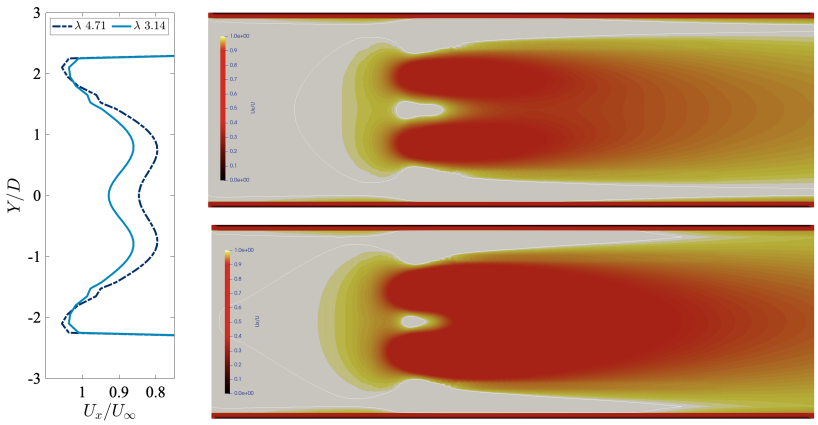


Figure 9: deficitVel

*5.2. The double rotor with surge motion*

The twin rotor was tested under two surge motions. The thrust force in Newton for both cases as a function of the surge period are included in: Fig. for a surge frequency, $f = 0.5$ Hz and a surge amplitude of $50mm$; and in Fig. (b) (b) with a surge frequency of 1Hz and an amplitude of $50mm$. For each case a total 20 periods were average with 500 bins. These experimental results were obtained without any type of filter, and because of the the complexity of rotating in addition to the surge motion, removing the noise resulted in the removing aerodynamic forces. Both cases where simulated by using $turbineFoam$ and the results are included in the same corresponding figures. For the case (a) The first case with $f = 1Hz$ allows 20 revolutions of the rotor per surge period. The induced velocity for this cases slightly modified the relative velocity, and hence, thrust force along the surge period depicted a constant pattern in the thrust behaviours for the 20 revolutions. This is observed in both the numerical and the experimental results. While most of the maximum values of the peak are well capture by the numerical simulations, the zero values expected at each 180 degrees of azimuthal angle, were capture for some instants during the surge motion. Therefore, since the induced velocity has a minimum effect in the $U_{rel}$ and the angle of attack, thus the second positive thrust observed detected by the measurement in the region where zero value were expected is associated to the harmonic influence of the surge and rotation frequencies.

The second case in Fig. (a) allow 10 rotations per surge period. For

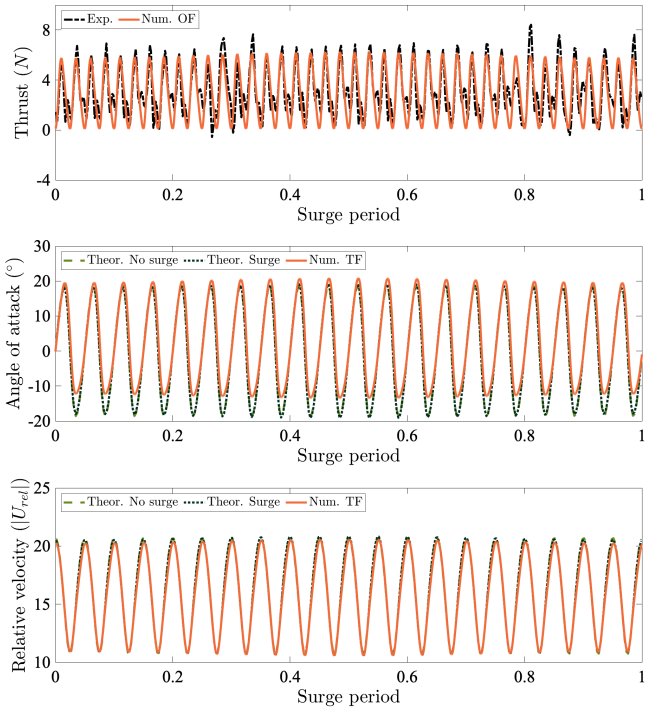


Figure 10: (a) Thrust force coefficient for the twin rotor, (b) Angle of attach and, (c) Magnitude of the relative velocity with $f = 0.5Hz$

these case, the influence of the induced velocity due to the surge motion is more notable for both experimental and numerical simulations. Again a positive thrust is observed with the experimental results while a zero value is observed with the numerical tool. Similarly to the previous case, the maximum peak agrees with both techniques but value of zero thrust are not observed in the experimental results as expected numerically. Since in both cases, the tendency of the surge in the influence of the surge motion is observed to be capture in good agreement with the experimental tests. It is important to mention that, these type of unsteady motion represent a huge challenge and other techniques such as pressure scanner could provide information which is less affected by vibrations and harmonic frequencies due to the mechanical movement-devices and also, providing detail of the surge effect in the boundary layer when the aerofoil induced velocity impact first at the backward of the aerofoil.

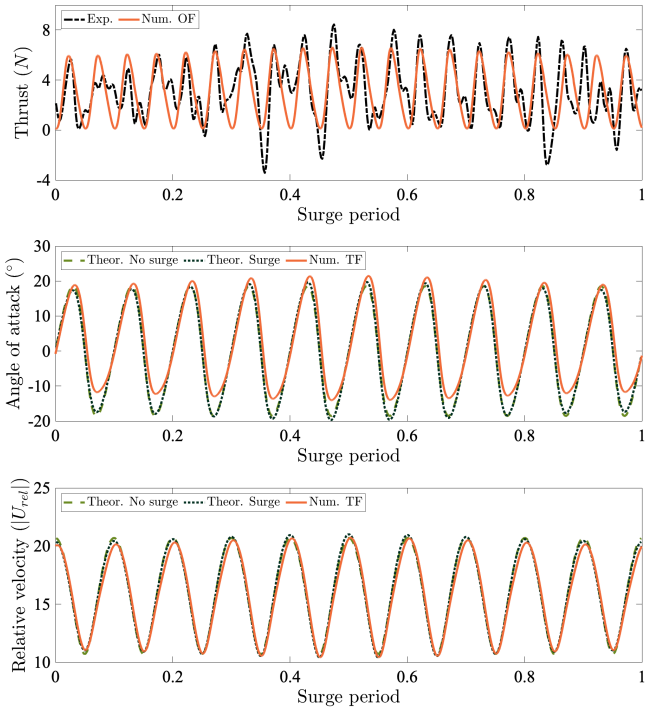


Figure 11: (a) Thrust force coefficient for the twin rotor, (b) Angle of attach and, (c) Magnitude of the relative velocity with $f = 1.0Hz$

### *5.3. Surge motion for a single rotor*

In order to assess the surge motion included in $TurbinesFoam$, the case 1, consisting in a 3D CFD simulation of a single VAWT undergoing a surge motion was investigated. The thrust force as a function of one period of surge is reported in [10]. This allows a detailed comparison of the thrust force predicted by using *turbinesFoam* (Num. OF-TF). The results included in Fig. 12 includes OF-TF prediction when using 3D losses for the ALM model and without 3D losses. There is a notorious over-prediction on the forces in general when 3D losses are not included but the effect of the surge, starting with low values of $T$ reaching a maximum value, and then decreasing again is in agreement with the full CFD case.

The results, when using the 3D losses showed a very good agreement with the CFD results.Despite that, the lower peaks observed in the CFD case are not properly capture by the OF-TF model. Accordingly to the available literature, the boundary layer conditions maybe affected mostly at

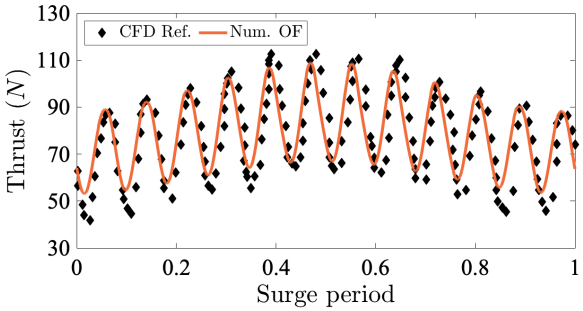


Figure 12: Comparison of the thrust force for a single rotor undergoing a surge motion with $f = 1.158$ and $X_m = 0.20m$.

the trailing edge of the aerofoil and this, affect the distribution of the pressure coefficient around the aerofoil and as a consequence the aerodynamic forces. The lower peak are observed at the beginning of the surge motion ( moving to the Right and the TE of the aerofoil being impacted by surge direction of the flow). In the region, from 0.25-0.75 this peaks are less severe; within this region the TE of the aerofoil perceives the velocity of the flow due to the surge and, from 0.75 to 1, when the rotor is moving to the right to return to its initial position, the TE might be affected again.

The relative velocity computed by the numerical method, OF-TF, is included in Fig. 13 and it is compared with theoretical relative velocity given by Eq. (10) for surge and without surge conditions. The two theoretical $U_{rel}$, with surge and without surge, indicted that under surge conditions, the velocity starts with the lower magnitude values (compared without surge), reached a maximum at half period and then, decreases again. This is due to the surge induced velocity that reduces $U_{rel}$ accordingly to Eqs. (1) and (2). The velocity, $U_{rel}$ computed by OF-TF, followed the same tendency that the theoretical $U_rel$ but the magnitude is smaller. This is related to the number of blades, three, of the rotor, and, TF-OF is able to take into account the deficit in the velocity due to the number of blades at both, upstream and downstream of the rotor. At downstream of the rotor, the effect of the number of blades becomes more significant and this is evident by observing the angle of attack in Fig. 13(b) where at downstream, the angle of attack halved regarding the theoretical values. It is important to emphasize, the unsteady aerodynamics that includes, surge, pitching, flapping, and other dynamics motion of aerofoils is not very well investigated yet when a combination of

unsteady motion occurs at the same time over the aerofoil. As a consequence, to verify numerical tools, including full CFD simulations, much more efforts in experiment concerning unsteady aerodynamics must be done.

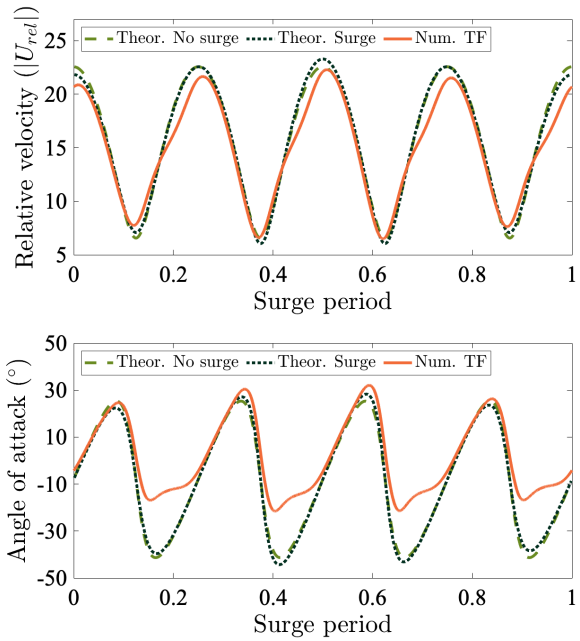


Figure 13: (a) Domain boundary conditions and (b) Representation of the computational subdomains:S, first subdomain and T, second subdomain surrounding the rotors.

This simulation had a number of $0.2 \times 5$ cells, and a total of 1.0 Hrs. computer clock time was employed to perform three surge periods.

## 6. Conclusions

- The new experimental data from a twin rotor VAWT has allowed assessing the capabilities of the modified *turbineFoam* model to predict the thrust force for this double rotor configuration and, under both fixed and floating conditions.

- The assessed numerical tool has the capabilities to investigate multiple rotors under floating off-shore conditions with a high level of confidence and low computational resources.

- The optimum domain dimensions, the size mesh, time step and surge periods have been stated and this can be used as a guideline to perform future simulations.

## References


[1] I. P. on Climate Change, Climate change 2022: Sixth assessment report, IPCC, 2022.

[2] I. E. Agency, World Energy Outlook 2022, IEA, 2022.

[3] X. Sun, D. Huang, G. Wu, The current state of offshore wind energy technology development, Energy 41 (1) (2012) 298–312.

[4] M.-K. Lee, J. Nam, M. Kim, Valuing the public preference for offshore wind energy: The case study in south korea, Energy (2022) 125827.

[5] B. Bulder, S. Krishna Swamy, P. Warnaar, I. Maassen van den Brink, M. de la Vleter, Pathways to potential cost reductions for offshore wind energy, TNO 2020 R11926, TNO inovation for life, 2020.

[6] A. Arredondo-Galeana, F. Brennan, Floating offshore vertical axis wind turbines: opportunities, challenges and way forward, Energies 14 (23) (2021) 8000.

[7] C. Matoug, B. Augier, B. Paillard, G. Maurice, C. Sicor, S. Barre, An hybrid approach for the comparison of vawt and hawt performances for floating offshore wind turbines, Journal of Physics: Conference Series 1618 (032026) (2020). doi:doi:10.1088/1742-6596/1618/3/032026.

[8] M. Guilbot, S. Barre, G. Balarac, C. Bonamy, N. Guillaud, A numerical study of vertical axis wind turbine performances in twin-rotor configurations, Journal of Physics: Conference Series 1618 (052012) (2020). doi:doi:10.1088/1742-6596/1618/5/052012.

[9] J.-L. Achard, G. Maurice, G. Balarac, S. Barre, Floating vertical axis wind turbine — owlwind project, in: 2017 International Conference on ENERGY and ENVIRONMENT (CIEM), 2017, pp. 216–220. doi:10.1109/CIEM.2017.8120794.

[10] H. Lei, D. Zhou, Y. Bao, C. Chen, N. Ma, Z. Han, Numerical simulations of the unsteady aerodynamics of a floating vertical axis wind turbine in surge motion, Energy 127 (2017) 1–17. doi:https://doi.org/10.1016/j.energy.2017.03.087.

[11] H. Lei, D. Zhou, J. Lu, C. Chen, Z. Han, Y. Bao, The impact of pitch motion of a platform on the aerodynamic performance of a floating vertical axis wind turbine, Energy 119 (2017) 369–383. doi:https://doi.org/10.1016/j.energy.2016.12.086.

[12] D. T. Griffith, M. F. Barone, J. Paquette, B. C. Owens, D. L. Bull, C. Simao-Ferriera, A. Goupee, M. Fowler, Design studies for deep-water floating offshore vertical axis wind turbines., Tech. rep., Sandia National Lab.(SNL-NM), Albuquerque, NM (United States) (2018).

[13] Z. Cheng, H. A. Madsen, Z. Gao, T. Moan, Effect of the number of blades on the dynamics of floating straight-bladed vertical axis wind turbines, Renewable Energy 101 (2017) 1285–1298. doi:https://doi.org/10.1016/j.renene.2016.09.074.

[14] H. Lei, J. Su, Y. Bao, Y. Chen, Z. Han, D. Zhou, Investigation of wake characteristics for the offshore floating vertical axis wind turbines in pitch and surge motions of platforms, Energy 166 (2019) 471–489. doi:https://doi.org/10.1016/j.energy.2018.10.101.

[15] L. Kuang, Q. Lu, X. Huang, L. Song, Y. Chen, J. Su, Z. Han, D. Zhou, Y. Zhao, Y. Xu, Y. Liu, Characterization of wake interference between two tandem offshore floating vertical-axis wind turbines: Effect of platform pitch motion, Energy Conversion and Management 265 (2022) 115769. doi:https://doi.org/10.1016/j.enconman.2022.115769.

[16] D. D. Tavernier, C. S. Ferreira, A new dynamic inflow model for vertical-axis wind turbines, Wind energy 23 (2020) 1196–1209. doi:https://doi.org/10.1002/we.2480.

[17] S. AD, The SeaTwirl concept.
URL `https://seatwirl.com/products/`

[18] Y. Jiang, P. Zhao, T. Stoesser, K. Wang, L. Zou, Experimental and numerical investigation of twin vertical axis wind turbines with

a deflector, Energy Conversion and Management 209 (2020) 112588. doi:https://doi.org/10.1016/j.enconman.2020.112588.

[19] A. Vergaerde, T. De Troyer, J. Kluczewska-Bordier, N. Parneix, F. Silvert, M. Runacres, Wind tunnel experiments of a pair of interacting vertical-axis wind turbines, in: Journal of Physics: Conference Series, Vol. 1037, IOP Publishing, 2018, p. 072049.

[20] A. Rezaeiha, H. Montazeri, B. Blocken, Towards accurate cfd simulations of vertical axis wind turbines at different tip speed ratios and solidities: Guidelines for azimuthal increment, domain size and convergence, Energy Conversion and Management 156 (2018) 301–316. doi:https://doi.org/10.1016/j.enconman.2017.11.026.

[21] G. Jin, Z. Zong, Y. Jiang, L. Zou, Aerodynamic analysis of side-by-side placed twin vertical-axis wind turbines, Ocean Engineering 209 (2020) 107296.

[22] A. Posa, Wake characterization of coupled configurations of vertical axis wind turbines using large eddy simulation, International Journal of Heat and Fluid Flow 75 (2019) 27–43.

[23] H. Lam, H. Peng, Study of wake characteristics of a vertical axis wind turbine by two- and three-dimensional computational fluid dynamics simulations, Renewable Energy 90 (2016) 386–398. doi:https://doi.org/10.1016/j.renene.2016.01.011.

[24] A. Alaimo, A. Esposito, A. Messineo, C. Orlando, D. Tumino, 3d cfd analysis of a vertical axis wind turbine, Energies 8 (4) (2015) 3013–3033. doi:10.3390/en8043013.

[25] B. Hand, Three-dimensional computational fluid dynamic analysis of a large-scale vertical axis wind turbine, Wind Engineering 0 (0) (2021) 0309524X211037911. doi:10.1177/0309524X211037911.

[26] F. Balduzzi, D. Marten, A. Bianchini, J. Drofelnik, L. Ferrari, M. S. Campobasso, G. Pechlivanoglou, C. N. Nayeri, G. Ferrara, C. O. Paschereit, Three-Dimensional Aerodynamic Analysis of a Darrieus Wind Turbine Blade Using Computational Fluid Dynamics and Lifting Line Theory, Journal of Engineering for Gas Turbines and Power 140 (2), 022602 (10 2017). doi:10.1115/1.4037750.

[27] K. H. Wong, W. T. Chong, S. C. Poh, Y.-C. Shiah, N. L. Sukiman, C.-T. Wang, 3d cfd simulation and parametric study of a flat plate deflector for vertical axis wind turbine, Renewable Energy 129 (2018) 32–55. doi:https://doi.org/10.1016/j.renene.2018.05.085.

[28] M. M. Elsakka, D. Ingham, L. Ma, M. Pourkashanian, Comparison of the computational fluid dynamics predictions of vertical axis wind turbine performance against detailed pressure measurements, International Journal of Renewable Energy Research 11 (1) (2021) 276–293. doi:https://doi.org/10.20508/ijrer.v11i1.11755.g8131.

[29] M. Elkhoury, T. Kiwata, E. Aoun, Experimental and numerical investigation of a three-dimensional vertical-axis wind turbine with variable-pitch, Journal of Wind Engineering and Industrial Aerodynamics 139 (2015) 111–123. doi:10.1016/j.jweia.2015.01.004.

[30] T. Maeda, Y. Kamada, J. Murata, T. Kawabata, K. Shimizu, T. Ogasawara, A. Nakai, T. Kasuya, et al., Wind tunnel and numerical study of a straight-bladed vertical axis wind turbine in three-dimensional analysis (part ii: For predicting flow field and performance), Energy 104 (2016) 295–307.

[31] J. Guo, L. Lei, Flow characteristics of a straight-bladed vertical axis wind turbine with inclined pitch axes, Energies 13 (23) (2020) 6281.

[32] P. Bachant, A. Goude, M. Wosnik, Actuator line modeling of vertical-axis turbines (2016). doi:10.48550/ARXIV.1605.01449.
URL `https://arxiv.org/abs/1605.01449`

[33] D. D. Tavernier, C. Ferreira, A. Li, U. Paulsen, H. Madsen, Towards the understanding of vertical-axis wind turbines in double-rotor configuration., Journal of Physics: Conference Series 1037 (2018) 022015. doi:10.1088/1742-6596/1037/2/022015.

[34] Z. Cheng, H. A. Madsen, Z. Gao, T. Moan, Aerodynamic modeling of floating vertical axis wind turbines using the actuator cylinder flow method, Energy Procedia 94 (2016) 531–543.

[35] B. LeBlanc, C. S. Ferreira, Estimation of blade loads for a variable pitch vertical axis wind turbine with strain gage measurements, Wind energy 25 (2022) 1030–1045. doi:https://doi.org/10.1002/we.2480.

[36] M. T. Nguyen, F. Balduzzi, A. Bianchini, G. Ferrara, A. Goude, Evaluation of the unsteady aerodynamic forces acting on a vertical-axis turbine by means of numerical simulations and open site experiments, Journal of Wind Engineering and Industrial Aerodynamics 198 (2020) 104093. doi:https://doi.org/10.1016/j.jweia.2020.104093.

[37] T. Maeda, Y. Kamada, J. Murata, K. Furukawa, M. Yamamoto, et al., Effect of number of blades on aerodynamic forces on a straight-bladed vertical axis wind turbine, Energy 90 (2015) 784–795.

[38] T. Maeda, Y. Kamada, J. Murata, K. Furukawa, M. Yamamoto, et al., The influence of flow field and aerodynamic forces on a straight-bladed vertical axis wind turbine, Energy 111 (2016) 260–271.

[39] P. Bachant, A. Goude, daa mec, M. Wosnik, turbinesFoam/turbinesFoam: v0.1.1, Zenodo, 2019. doi:10.5281/zenodo.3542301.
URL `http://www-cs-faculty.stanford.edu/ uno/abcde.html`

[40] O. Ltd., ESI OpenCFD Release OpenFOAM® v2106.
URL `https://www.openfoam.com/`

[41] O. Ltd., OpenFoam User guide v2112, Linear Eddy Viscocity models.
URL `https://www.openfoam.com/documentation/guides/`

[42] L. Daróczy, G. Janiga, K. Petrasch, M. Webner, D. Thévenin, Comparative analysis of turbulence models for the aerodynamic simulation of h-darrieus rotors, Energy 90 (2015) 680–690.

[43] A. Rezaeiha, H. Montazeri, B. Blocken, On the accuracy of turbulence models for cfd simulations of vertical axis wind turbines, Energy 180 (2019) 838–857.